Co-channel Interference Between WiFi and Through-Wall Micro-Doppler Radar

Akash Deep Singh, Shelly Vishwakarma and Shobha Sundar Ram
Dept. of Electronics and Communication Engineering
Indraprastha Institute of Information Technology Delhi
New Delhi, India 110020
{akash14131, shellyv, shobha}@iiitd.ac.in

***Abstract*—Narrowband through-wall radars have been researched for detecting and classifying indoor movers on the basis of their micro-Doppler signatures. These radars usually operate in the unlicensed 2.4GHz ISM band and are therefore susceptible to interference from WiFi networks operating with the IEEE 802.11g protocol. In this work, we show, through experiments, how the radar degrades the WiFi throughput by lowering the signal to noise and interference ratio at the WiFi receiver. Similarly, WiFi interference causes deterioration in the radar performance by increasing the probability of false alarms.**

I. Introduction

Through-wall radars have been researched and developed over the last decade for detecting and monitoring humans in urban environments [1]–[4]. The current radars are typically of two types - narrowband and broadband radars. Broadband radars provide range information of the humans [5], [6], while the narrowband radars provide Doppler information regarding moving humans in the presence of stationary background clutter [7], [8]. Narrowband radar returns of moving humans are characterized by micro-Doppler features arising from the motions of the arms and legs. These returns, when represented in the joint time-frequency space, have been demonstrated to be very effective for detecting and classifying different types of human motions [9]–[13] as well as distinguishing humans from other moving targets [14], [15]. The performance of radars, particularly of narrowband radars, are susceptible to degradation due to interference from neighborhood wireless sources. Most narrowband radars operate in the unlicensed 2.4GHz band [16]. The FCC regulations mandate that the maximum equivalent isotropic radiated power from any wireless device operating at 2.4GHz must be less than 1 Watt. This band is used by several wireless systems such as microwave ovens, baby monitors and the ubiquitous WiFi following the IEEE 802.11g protocol. The objective of this work is to study the co-channel interference between WiFi systems and narrowband micro-Doppler radars at 2.4GHz.

Research into issues related to co-existence of wireless communication systems and radar in the spectrum between 500MHz and 6GHz has recently gained significant interest. In 2003, the interference between military radars and WLAN networks were studied in [17]. In [18], the authors presented mechanisms to reduce the interference from local area networks on meteorological radars. More recently, the authors in [19] presented a detailed study of the impact of terrestrial radar on the throughput of WLAN networks. In all of the above instances, the radars have fixed locations and predictable behavior and hence present opportunities for minimizing the interference between the communication and radar systems. On the other hand, through-wall radars pose very different challenges. Through-wall radars are designed with an objective of surveillance for law enforcement operations. Hence, they are usually portable (positions are not fixed) and their performance should necessarily be unpredictable to the indoor occupants. Radar parameters such as the carrier frequency, transmitted waveform and power should be selected so as to minimize the possibility of detection by WiFi users. In [2], the authors investigated the possibility of using passive radar using scattered signals from WiFi to detect indoor movers. While the passive radar offers a very low probability of detection, the radar requires prior knowledge of the WiFi system configuration and layout. When such information is not readily available, through-wall active radars remain the only alternative for obtaining information regarding indoor movers.

In [20], we presented a method for detecting multiple indoor movers using a through-wall micro-Doppler radar based on dictionary learning. The main advantage of our radar over other micro-Doppler radars is that it has the capability of detecting more than one mover in the channel. Here, the radar learns unique dictionaries of the micro-Dopplers from different target motions from training data sets. Then a target belonging to a particular class is detected if the strength of the coefficient of the corresponding dictionary is above a predefined threshold. The strength of the coefficient is a function of both the match between the micro-Doppler signature of the test target and the trained signature as well as the magnitude of the received signal. The threshold is chosen so as to maximize the probability of detection (P_D) for a particular value of probability of false alarm (P_{FA}) for a given signal to noise ratio (SNR) of the radar receiver. The presence of interference sources can significantly impact the performance of such a system. In this work, we perform extensive experimental analysis to study the co-existence issues between the WiFi and through-wall radar when they jointly operate in the unlicensed 2.4GHz band. In particular, we detail how the presence of interference from WiFi affects the probability of detection and false alarm for the micro-Doppler radar. Additionally we also measure the impact of the radar on the throughput of the WiFi link. Our paper is organized as follows. In the following section, we provide the theory for interference between the micro-Doppler radar and the WiFi systems. In section III, we describe the experimental set up for measuring WiFi throughput and through-wall radar performance. Then we simulate the background noise and

978-1-4673-8823-8/17/$31.00 ©2017 IEEE

signal to interference and noise curves of the WiFi system for different radar powers. In Section IV, we present the measurement results and analysis. We conclude with the final section.

II. Theory

When a radar and WiFi system operate in the same channel (wavelength, λ), the performances of both systems are affected by mutual interference. Consider a single point to point WiFi communication link with the receiver at port 1 and transmitter at port 2 and a monostatic radar at port 3. In the case of the radar, P_D and P_{FA} are important metrics to measure the radar's performance. In pulse radar, a target is detected if the strength of the matched filter response of the scattered signal is above a preset threshold based on the SNR of the receiver. In continuous wave radars, we apply a similar criterion on the micro-Doppler signatures for detecting the presence of moving targets. Several works have represented micro-Doppler signatures with traditional transforms such as short time Fourier transform (STFT) and wavelets [9]. However, the transform parameters (such as dwell time duration in STFT) have to be carefully optimized for each particular type of target motion. Therefore, these transforms are inherently unsuitable for the detection of multiple simultaneous movers in the channel. In [20], we proposed using data derived dictionaries to represent micro-Dopplers from multiple targets. The dictionary learning (DL) algorithm, first introduced by [21], [22], generates a pool of signal vectors, D, from training micro-Doppler data, X, yielding a sparse representation, Z, as shown in (1).

$$X = DZ \tag{1}$$

The algorithm overcomes the limitations of off-the-shelf fixed dictionaries since it does not require heuristic feature extraction. The learning problem fundamentally minimizes the constrained Euclidean cost function $J(D, Z)$ as shown in (2).

$$J(D, Z) = \min_{D,Z} \|X - DZ\|_F^2 \, s.t. \, \|Z\|_0 \leq \beta \tag{2}$$

Here, Z is made β sparse using l_0 norm. Since l_0-minimization is an NP-hard problem [23], it is relaxed to a l_1-minimization problem [24] as shown in (3).

$$J(D, Z) = \min_{D,Z} \|X - DZ\|_F^2 + \gamma \|Z\|_1 \tag{3}$$

Here, $\gamma \in \Re$ is the regularization parameter that controls the tradeoff between sparsity and signal representation error. We refer readers to [20] for a more detailed description of the dictionary learning algorithm for a micro-Doppler radar. The test micro-Doppler data, $\tilde{X}$ is combined with the dictionary, D_c, of a target class, c, to generate $\tilde{Z}_c$. Target c is determined to be present in the channel if the strength of $||\tilde{Z}_c||_2$ is above a pre-defined threshold. Therefore, the detection of the target depends on the the strength of the coefficients $||\tilde{Z}||_2$ which is a function of two parameters-

1) the strength of the received signal $||\tilde{X}||_2$ since (1) is a linear transform
2) how well the test signature, $\tilde{X}$, matched the previously trained signature, X

The choice of the threshold of $||\tilde{Z}||_2$ is critical and is chosen so as to maximize P_D for a particular P_{FA} and SNR, $\frac{P_{33}}{Noise_3}$, of the through-wall monostatic radar receiver. Here, $Noise_3$ is the noise at the radar receiver and P_{33} is given by

$$P_{33} = \frac{P_3^{tx} G_3^2 (\theta, \phi) \sigma \lambda^2}{L^2 (4\pi)^3 R^4} \tag{4}$$

where P_3^{tx} is the transmitted power from the radar, σ is the radar cross-section of the target, L is the through-wall attenuation and G_3 is the gain of the transmitting and receiving antennas (assuming they have the same gain). When the radar is deployed in an urban environment where WiFi interference is present, the SINR at the receiver is given by $\frac{P_{33}}{P_{32}+Noise_3}$ where P_{32} is the interference from the WiFi transmitter. The strength of P_{32} will not be known since the radar operator is unlikely to have information regarding the WiFi configuration in the deployment scenario. Instead the threshold will be optimized based on laboratory measurements prior to deployment. As a result of which the P_{FA} and P_D may change significantly during operation.

In the case of WiFi, the throughput of the link is a good metric to measure the performance. The throughput is indirectly related to the SINR at the WiFi receiver, $\frac{P_{12}}{P_{13}+Noise_1}$. Here, P_{12} is the received power at port 1 from the transmitter at port 2; P_{13} is the interference from the radar and $Noise_1$ is the noise at the WiFi receiver. The received power, P_{nm}, at any port n from transmitter at port m can be estimated from the well known Frii's transmission equation provided the transmitted power (P_m^{tx}), the gains at both the ports (G_m, G_n) and the free space loss are known as shown in (5)

$$P_{nm} = \frac{P_m^{tx} G_m (\theta, \phi) G_n (\theta, \phi) \lambda^2}{L_{nm} (4\pi R)^2} \tag{5}$$

An additional term, L_{nm}, accounts for any type of loss in the communication link between ports n and m. This could be due to system losses such as impedance mismatch or polarization losses at the antennas or propagation losses in the medium. While the above equation generally holds for free space conditions, multipath in the propagation channel may significantly alter the rate of decay of the received power with distance.

III. Experimental Set Up

In order to study the co-channel interference between the through-wall radar and WiFi, joint radar and WiFi measurements are carried out in laboratory conditions shown in Fig.1. The experiments are conducted in a 29m x 3m corridor. The corridor is empty of furniture and the only multipath that can arise are reflections from the floor, ceiling and walls of the corridor. A WiFi communication link is set up between two nodes, port 1 (receiver) and port 2 (transmitter), in line-of-sight conditions as indicated by the red and black pointers on the figure. The radar is deployed behind a 29cm brick wall at port 3. A human subject walks before the radar on the other side of the wall (within the corridor) as indicated by the dotted arrow. Besides the radar and the WiFi link, there are three other WLAN access points mounted on the ceiling of the corridor at 3m, 17m and 27m. There are three similarly placed access points on the two floors below. These floors are identical to the top floor in terms of layout and furniture. The radiations from these access points give rise to background noise in both the radar and WiFi measurements.

978-1-4673-8823-8/17/$31.00 ©2017 IEEE

A. WiFi Link

A line-of-sight WiFi communication link is setup between two laptops with Intel Centrino advanced-N 6205 wireless adapters. The antennas on these adapters are omnidirectional and of low gain (1-2dBi). The transmitted power is $15dBm$. Hostpad, a daemon for 802.11 access point management, is installed in one of the laptops which is hitherto referred to as the host (port 1). We configure the host as a IEEE 802.11g WiFi hotspot. Orthogonal frequency division multiplexing with quadrature phase-shift keying (QPSK) modulation scheme is implemented with a maximum raw data rate of 54Mbps on channel 11 that corresponds to 2.462 GHz subcarrier frequency. We set up iPerf on the host for monitoring the quality of the performance of the wireless communication link. After initial configuration, the host sends beacons to the client (port 2) to set up the link. Subsequently, the client sends 100M UDP data packets to the host over a duration of 27s. These packets are received by the host which publishes the throughput of the communication every second. The host therefore, can be referred to as the receiver and the client as the transmitter. The receiver is placed at port 1 whose position is fixed. The transmitter is placed at port 2 whose position is varied across the length of the room over 1m intervals as indicated by the green dots in Fig.1. Therefore, the receiver is always within the field-of-view (FOV) of the radar antennas while the transmitter moves out of the FOV of the radar antennas once it is beyond 5m. The throughput is measured when the radar is off and when the radar is transmitting power of $-15dBm$, $-5dBm$ and $+3dBm$.

B. Through-Wall Micro-Doppler Radar

A monostatic continuous wave radar is operated at 2.462 GHz as shown in Fig.2 behind a 29cm indoor brick wall. The radar system consists of a N9926A FieldFox vector network analyzer (VNA) and two linearly polarized double ridged horn antennas (HF907) separated by a distance of 30cm. Time domain S_{21} measurements of the VNA capture the back-scattered radar returns from a human test subject who walked on the other side of the wall (inside the long corridor) as shown in Fig.1.The human subjects moved roughly between 1m and 7m. The duration of each measurement was 27s with a sampling frequency of 370Hz. We measured radar returns at three radar transmitter power levels - $+3$dBm, -5dBm and -15dBm in both the presence and absence of the WiFi link, described above.

C. Simulation of Background Noise

The performance of the both the radar and WiFi systems are affected by background noise consisting of radiation from other access points in the building. Since, these signals are time-varying and depend on multiple factors (number of users, network level protocols etc.), we model their interference using Monte Carlo simulations. The following assumptions are made for the simulation. For each realization, the transmitted power from each of the access points is randomly chosen from $-1dBm$ to $+20dBm$; the distance of the access points from the receiver of the WiFi link (port 1) is varied from 1m to 40m and loss is varied from $0dB$ to $-40dB$. The system loss includes the effect of propagation loss through the floors, the degree of co-channel interference between the access points

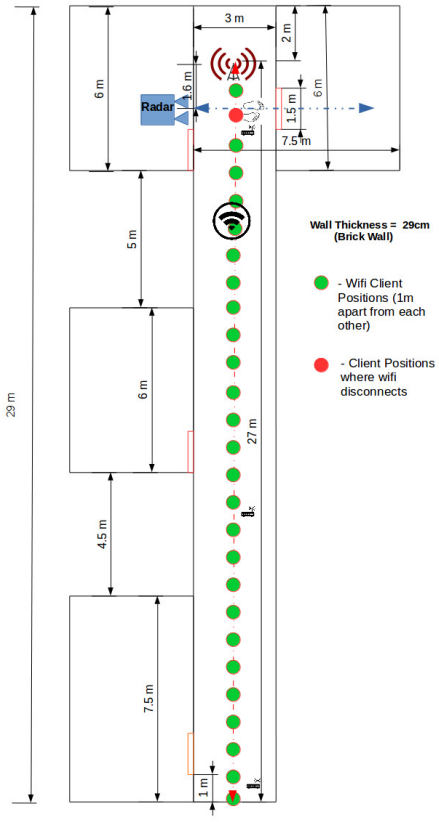

Fig. 1. Experimental set up of joint measurement data collection of through-wall radar scatterings from moving human and WiFi communication system in laboratory conditions

Fig. 2. Monostatic continuous wave through-wall radar configured using vector network analyzer and two horn antennas.

and the link as well as other system losses. In all of the cases, the gains of the antennas on the access points are assumed to be $0dBi$. Then, we compute the received power on the WiFi link (background noise) for each realization using the Frii's transmission equation in (5). We plot the distribution of the noise as a function of its strength in Fig.3. The figure shows a distribution with a mean noise (μ) of $-66dBm$ with a standard deviation (σ) of $8.5dBm$.

Next, we estimate the SINR of the WiFi receiver for different distances between the transmitter (port 1) and receiver (port 2). As mentioned earlier, the port 2 remains fixed as shown in Fig.1. However, port 1 is moved across the green positions at intervals of 1m. The SINR of the WiFi link is estimated using (5) for three different radar powers and when

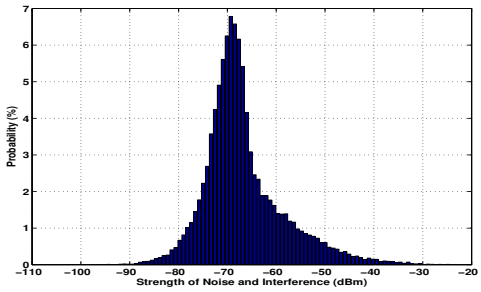

Fig. 3. Histogram of background noise due to interference from other access points in the building

the radar is off ($P_{23} = 0W$). In each case, we compute the SINR using the mean noise from Fig.3 as well as values corresponding to $\mu \pm \sigma$. The results are shown in Fig.4. As expected, the SINR is a function of both the distance between the transmitter and receiver ports as well as the radar interference.

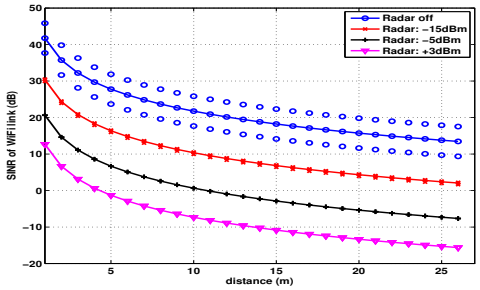

Fig. 4. Signal to interference and noise ratio (SINR) of the WiFi link for different distances between transmitter and receiver. Interference arises from the through-wall radar.

IV. Measurement Results and Analysis

In this section, we describe the measurement results obtained from the experiments. The first set of results demonstrate the effect of radar interference on WiFi throughput while the second set show the effect of WiFi on the radar's P_D and P_{FA}.

A. Effect of Through-wall Radar on WiFi Throughput

The throughput of the WiFi link is measured at the WiFi receiver as the distance between the transmitter and receiver ports is varied and for different radar powers. The results are shown in Fig.5. The results indicate that the throughput is directly related to the SINR at the receiver. In the absence of radar interference, the value of throughput is very high and almost constant at 28Mbps right from 1m to 26m in Fig.5(a). When the radar is switched on, the throughput falls with increasing distance between the ports. The throughput falls rapidly, to as low as a few Kbps (Fig.5(d), when the radar power is $+3dBm$. The box-cars in the plots show the variation in the measured throughput in each instance possibly due to the corresponding variation in the background noise. There is an aberration when the transmitter is at distances 2m and 3m from the receiver where a high fall in through-put is observed in Fig.5(b) and Fig.5(c). This is because, the transmitter of the WiFi (port 2) is in the FOV of the radar. As mentioned earlier, the transmitter is the client in the WiFi configuration while the receiver is the host. The host sends initial beacons to the client to set up the link, subsequent to which the client sends communication packets (which are used to calculate the throughput). Due to the high interference between the beacons and radar signals at the client, the link is often disconnected and this causes a significant fall in the throughput. Once the port 2 is outside the FOV of the radar, this problem ceases to affect the WiFi performance. In Table.I, we correlate the throughput results with the approximate SINR shown in Fig.4. Note that the throughput drops drastically (over 50%) when the SINR falls below $0dB$. With the drop in throughput, the supported WiFi services will also be affected. Table.II shows the different WiFi services and their throughput requirements. This table indicates that the WiFi user may become *aware* of the disturbance due to the radar based on the service that he is availing.

TABLE I. SINR vs Throughput Drop

Throughput drops by	SINR (dB)
100%	-6
75%	-4
50%	0
25%	8

TABLE II. WiFi throughput required for different modes of communication

Use	Required	Recommended
VoIP Calls	64Kbps	90Kbps
Video Calls	1.2Mbps	1.5Mbps
Group Video Calls	4Mbps	8Mbps
Live Video Streaming	3Mbps (SD)	5Mbps (HD)

B. Effect of WiFi on Through-Wall Radar Performance

We use STFT for generating the micro-Doppler spectrograms, from measurement data captured from a human walking behind the brick wall, as shown in Fig.6. The periodicity in the Dopplers in the spectrogram corresponds to the gait of the human. The Doppler spread is a function of the velocity and height of the human since the feet give rise to the maximum absolute values of Dopplers. Figs.6(a) and 6(c) show the spectrograms corresponding to two different radar powers in the absence of WiFi interference. We observe that the SNR is lower when the radar power is lower. When the radar power is high ($+3dBm$), the introduction of the interference source does not significantly distort the micro-Doppler signatures as shown in Fig.6(b). But when the transmitted power from radar is lowered to -15dBm, we can see a noticeable rise of the noise floor due to interference as seen in Fig.6(d). In particular, we observe that the micro-Dopplers of the arms and legs are most strongly affected by the noise rather than the strong torso returns. This is likely to affect the detection of the target since the detection is based on both the strength of the scattered signal as well as the match between the test and trained micro-Doppler signatures.

As discussed in Section II, the radar detection is based on whether the strength of the dictionary coefficients of the test data is above a pre-set threshold. Fig.7 shows the histogram of strength of $||Z||_2$ obtained for four cases. Each histogram

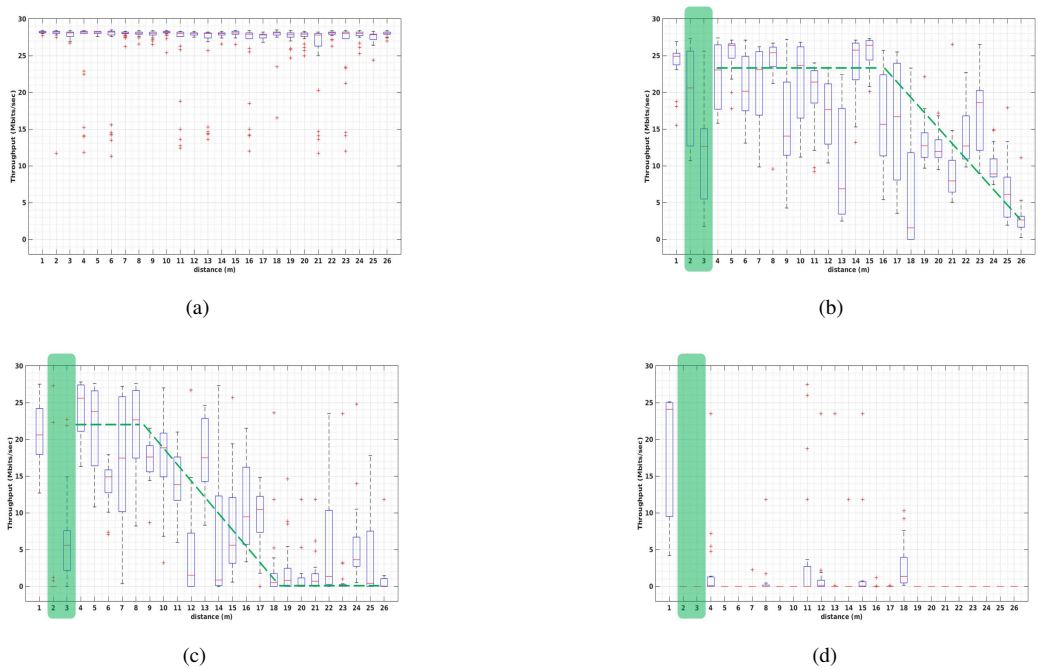

(a) (b) (c) (d)

Fig. 5. Throughput of the WiFi communication system when (a) when the through-wall radar is switched off and when the radar transmits (b) $-15dBm$ power, (c) $-5dBm$ and (d) $+3dBm$.

is drawn from 26 radar measurements. The first histogram is obtained from measurements made in the absence of both target and WiFi interference (*N*). The second histogram is generated when a human target is present but there is no WiFi interference (*S+N*). The threshold for $||Z||_2$ is selected to minimize P_{FA} and maximize P_D. Here, P_{FA} is the cumulative density in the *N* histogram above the threshold value and P_D is the cumulative density in the *S+N* histogram above the threshold. When the WiFi interference is present, both of these curves shift to the right as shown in the figure resulting in (*N+I*) and (*S+N+I*) histograms. This shift can be attributed to the increase in the strength of the scattered signal, $||X||_2$. However, the threshold remains unchanged. The P_{FA} and P_D are estimated for the radar in the presence and absence of the WiFi interference and the results are presented in Table.III for three different radar powers ($+3dBm, -5dBm$ and $-15dBm$). While P_D only slightly changes, we observe a very significant rise (above 40%) in P_{FA} for all three cases.

TABLE III. PROBABILITY OF DETECTION AND FALSE ALARM FOR MICRO-DOPPLER RADAR IN THE PRESENCE OF WIFI INTERFERENCE

	WiFi Off		**WiFi On**	
Radar Power (dBm)	P_{fa} %	P_d %	P_{fa} %	P_d %
-15	11	90	65	96
-5	13	90	61	93
$+3$	23	90	65	93

V. CONCLUSION

When the SINR of a WiFi receiver falls below -6dB due to the interference introduced by a co-channel narrowband through-wall radar at 2.4GHz, the throughput of the link falls by nearly 100%. Similarly, WiFi causes the radar performance to deteriorate. The probability of false alarm at the radar receiver increases by over 40% due to co-channel WiFi interference from a single link. Since the radar is mostly used for surveillance purposes, it is unlikely that the two systems will collaborate to minimize their co-channel interference.

ACKNOWLEDGMENT

The authors would like to thank Dr. Sanjit Kaul for his assistance in setting up the WiFi network and Dr. Sumit Roy for the valuable discussions.

REFERENCES

[1] S. S. Ram, C. Christianson, Y. Kim, and H. Ling, "Simulation and analysis of human micro-dopplers in through-wall environments," *IEEE Transactions on Geoscience and remote sensing*, vol. 48, no. 4, pp. 2015–2023, 2010.

[2] K. Chetty, G. E. Smith, and K. Woodbridge, "Through-the-wall sensing of personnel using passive bistatic wifi radar at standoff distances," *IEEE Transactions on Geoscience and Remote Sensing*, vol. 50, no. 4, pp. 1218–1226, 2012.

[3] G. Wang and M. G. Amin, "Imaging through unknown walls using different standoff distances," *IEEE Transactions on Signal Processing*, vol. 54, no. 10, pp. 4015–4025, 2006.

[4] M. G. Amin, *Through-the-wall radar imaging*. CRC press, 2016.

[5] J. Marcum, "A statistical theory of target detection by pulsed radar," *IRE Transactions on Information Theory*, vol. 6, no. 2, pp. 59–267, 1960.

[6] D. R. Wehner, "High resolution radar," *Norwood, MA, Artech House, Inc., 1987, 484 p.*, vol. 1, 1987.

[7] J. L. Geisheimer, E. F. Greneker III, and W. S. Marshall, "High-resolution doppler model of the human gait," in *AeroSense 2002*. International Society for Optics and Photonics, 2002, pp. 8–18.

[8] F.-k. Li, D. N. Held, J. C. Curlander, and C. Wu, "Doppler parameter estimation for spaceborne synthetic-aperture radars," *IEEE transactions on geoscience and remote sensing*, no. 1, pp. 47–56, 1985.

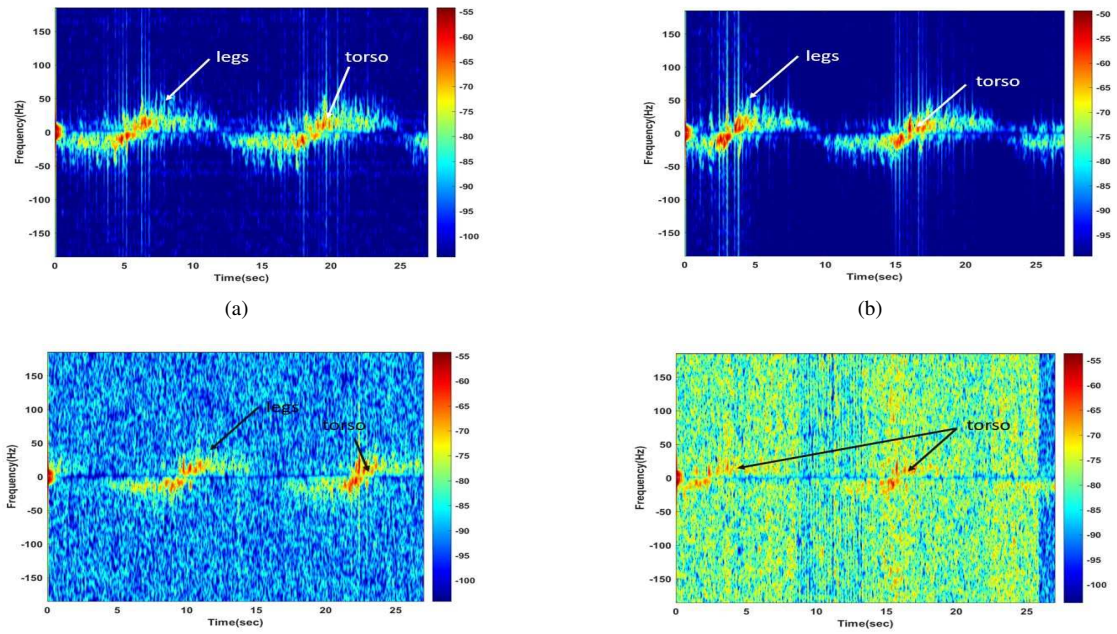

Fig. 6. Micro-Doppler signatures of a human walking to and fro on the other side of the wall to the radar when (a) radar transmits 3dBm power and WiFi is off, (b) radar transmits 3dBm power and WiFi is on, (c) radar transmits -15dBm power and WiFi is off, and (d) radar transmits -15dBm power and WiFi is on.

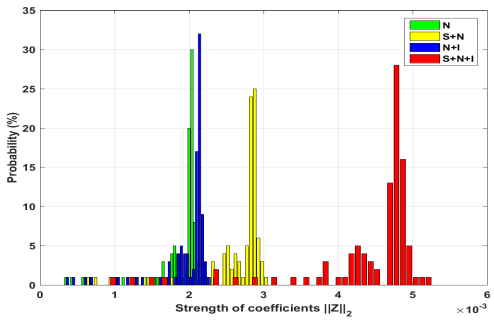

Fig. 7. Histogram of dictionary coefficient for detection of micro-Doppler target under noise (target absent, WiFi off); noise and interference (target absent, WiFi on); signal and noise (target present, WiFi off); and signal and noise and interference (target present, WiFi on) conditions.

[9] V. C. Chen, "Analysis of radar micro-doppler with time-frequency transform," in *Statistical Signal and Array Processing, 2000. Proceedings of the Tenth IEEE Workshop on*. IEEE, 2000, pp. 463–466.

[10] V. C. Chen, F. Li, S.-S. Ho, and H. Wechsler, "Micro-doppler effect in radar: phenomenon, model, and simulation study," *IEEE Transactions on Aerospace and Electronic systems*, vol. 42, no. 1, pp. 2–21, 2006.

[11] B. Lyonnet, C. Ioana, and M. G. Amin, "Human gait classification using microdoppler time-frequency signal representations," in *2010 IEEE Radar Conference*. IEEE, 2010, pp. 915–919.

[12] I. Orović, S. Stanković, and M. Amin, "A new approach for classification of human gait based on time-frequency feature representations," *Signal Processing*, vol. 91, no. 6, pp. 1448–1456, 2011.

[13] B. G. Mobasseri and M. G. Amin, "A time-frequency classifier for human gait recognition," in *SPIE Defense, Security, and Sensing*. International Society for Optics and Photonics, 2009, pp. 730 628–730 628.

[14] T. Thayaparan, L. Stanković, and I. Djurović, "Micro-doppler-based target detection and feature extraction in indoor and outdoor environments," *Journal of the Franklin Institute*, vol. 345, no. 6, pp. 700–722, 2008.

[15] M. G. Amin, F. Ahmad, Y. D. Zhang, and B. Boashash, "Human gait recognition with cane assistive device using quadratic time–frequency distributions," *IET Radar, Sonar & Navigation*, vol. 9, no. 9, pp. 1224–1230, 2015.

[16] A. Lin and H. Ling, "Doppler and direction-of-arrival (ddoa) radar for multiple-mover sensing," *IEEE transactions on aerospace and electronic systems*, vol. 43, no. 4, pp. 1496–1509, 2007.

[17] D. Leiss, "Co-interference between military radars and 802.11 a wlan networks," in *AUTOTESTCON 2003. IEEE Systems Readiness Technology Conference. Proceedings*. IEEE, 2003, pp. 290–293.

[18] Z. Horváth and D. Varga, "Channel allocation technique for eliminating interference caused by rlans on meteorological radars in 5 ghz band," *Infocommunications Journal*, vol. 64, no. 3, pp. 24–34, 2009.

[19] F. Hessar and S. Roy, "Spectrum sharing between a surveillance radar and secondary wi-fi networks," *submitted to IEEE Transactions on Aerospace and Electronic Systems*, pp. 1–26, 2016.

[20] S. Vishwakarma and S. S Ram, "Detection of multiple movers based on single channel source separation of their micro-dopplers," *submitted to IEEE Transactions on Aerospace and Electronic Systems*, 2016.

[21] J. Mairal, J. Ponce, G. Sapiro, A. Zisserman, and F. R. Bach, "Supervised dictionary learning," in *Advances in neural information processing systems*, 2009, pp. 1033–1040.

[22] Q. Zhang and B. Li, "Discriminative k-svd for dictionary learning in face recognition," in *Computer Vision and Pattern Recognition (CVPR), 2010 IEEE Conference on*. IEEE, 2010, pp. 2691–2698.

[23] B. K. Natarajan, "Sparse approximate solutions to linear systems," *SIAM journal on computing*, vol. 24, no. 2, pp. 227–234, 1995.

[24] I. W. Selesnick and I. Bayram, "Sparse signal estimation by maximally sparse convex optimization," *IEEE Transactions on Signal Processing*, vol. 62, no. 5, pp. 1078–1092, 2014.